Cell Reports
Physical Science

Article

Rotational energy harvesting for automotive applications using coiled carbon nanotube yarn

Graphical abstract

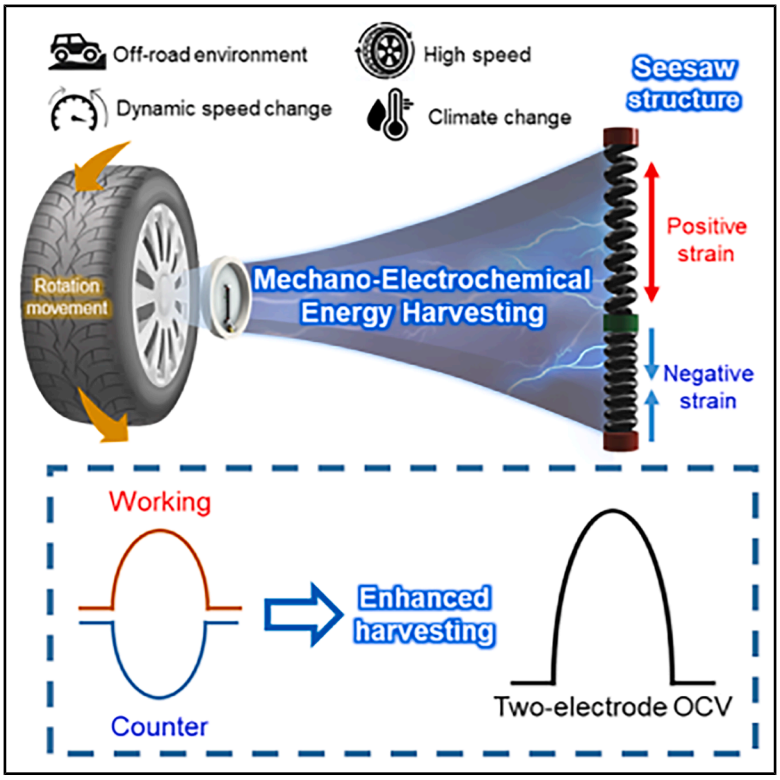

Highlights

- Seesaw-structured CNT yarn-based rotational harvester boosts energy harvesting performance
- Rotational harvester based on CNT shows high durability in real-auto-like environments
- Energy storage application at high speed shows suitability for automobile energy harvester

Authors

Ji Hwan Moon, Bum-Joon Kim, Yongwoo Jang, ..., Tae Jin Mun, Danyoung Kim, Seon Jeong Kim

Correspondence

sjk@hanyang.ac.kr

In brief

A high-durability rotational energy harvester uses electrochemical capacitance changes of coiled CNT yarn with a one-body seesaw structure to enhance harvesting by alternately stretching and releasing the electrodes. Moon et al. demonstrate stable performance under automotive-like environmental conditions and high rotational speeds, enabling practical energy storage for vehicle applications.

Moon et al., 2026, Cell Reports Physical Science 7, 103263
May 20, 2026 © 2026 Published by Elsevier Inc.
https://doi.org/10.1016/j.xcrp.2026.103263

CellPress

Cell Reports
Physical Science

CellPress
OPEN ACCESS

Article

Rotational energy harvesting for automotive applications using coiled carbon nanotube yarn

Ji Hwan Moon,[1,3] Bum-Joon Kim,[1,3] Yongwoo Jang,[1,2] Gyu Hyeon Song,[1] Sumin Yoon,[1] Tae Jin Mun,[1] Danyoung Kim,[1] and Seon Jeong Kim[1,4,*]

[1]Department of Biomedical and Electronic Engineering, Hanyang University, Seoul 04763, South Korea
[2]Department of Pharmacology, College of Medicine, Hanyang University, Seoul 04736, South Korea
[3]These authors contributed equally
[4]Lead contact
*Correspondence: sjk@hanyang.ac.kr
https://doi.org/10.1016/j.xcrp.2026.103263

SUMMARY

A rotational energy harvester converts rotational motion into mechanical deformation to generate electrical energy and is important for automotive applications. However, practical use requires stable energy harvesting under varying driving conditions, including changes in speed, temperature, and humidity. Here, we report a rotational energy harvester based on electrochemical capacitance changes of coiled carbon nanotube (CNT) yarn in a solid electrolyte under mechanical strain. A seesaw structure simultaneously stretches one electrode while releasing the other, enhancing performance. The device converts wheel rotation into linear stretching of coiled CNT yarn and operates under dynamic speed variations, high speed (~1,500 rpm), and environmental changes (20°C–60°C, 40%–80% humidity). When connected to a boost converter, it generates a peak voltage of 4.8 V and charges a capacitor up to 4.2 V, demonstrating suitability for practical automotive applications.

INTRODUCTION

In the industrial, robotic, and biomedical fields, the need for the advanced development of compact sustainable power supplying systems has grown with wearable devices and smart electronic devices.[1–6] Remarkably, an energy harvester, which harvests energy from ambient energy from the system's environment, is emerging as a way of replacing conventional energy supply systems based on batteries, which have concerns regarding large volumes, limited battery life causing the inconvenience of replacement, and environmental pollution caused by discarded batteries.[7–12]

Among the various energy harvesting methods, mechanical energy harvesting has been a key technical component in various applicable fields where kinetic movements are abundant and power supplements are required.[13,14] In particular, the energy generated by rotational movements is an important energy harvesting source that is frequently found in our lives.[15] Therefore, rotational energy harvesters (REHs) are widely used to harvest electrical energy from mechanical energy derived from rotating devices,[16,17] human motions,[18,19] and ambient environments such as the fluid flow of wind[20–28] and water.[29,30] In particular, because of the ubiquitous use of various rotary machines and wheel devices, harvesting energy from direct rotational motion of devices has become important.[16] In terms of automobile energy harvester, REH is regarded as the most efficient and reliable solution since the car wheels continuously roll on roads while driving, and its features are independent of external environmental factors.[13,31]

Although there are some automobile rotational harvesters challenging to improve the stable performance in high-speed regions (>500 rpm), unstable power generated during speed changes and humidity changes, other research shows wide frequency bandwidth with volumetric high power density as rotational harvesting applications including automobile rotational harvesters.[32–40]

In recent years, an energy harvesting technology was developed, which converts tensile mechanical energy to electrical energy due to stretch-induced capacitance changes of a coiled carbon nanotube (CNT) yarn,[41] which is made from the twisting and tensioning of the CNT sheet.[42,43] The coiled CNT yarn harvester can convert tensile or torsional oscillation into electrical energy without bias voltage, unlike other harvesters. This CNT yarn has great mechanical properties for dynamic deformation with fast speeds in that stretching a coiled CNT yarn generates an open-circuit voltage (OCV) and electrical power within 30 Hz of frequency in proportion to the strain deformation of the CNT yarn. In addition, the compact structure of coiled yarn has versatility for many application fields and exhibits outstanding harvesting performance with high gravimetric power density, showing various applications such as wearable harvesters and self-powered sensors.[44–51] Therefore, a coiled CNT yarn harvester has remarkable advantages such as high mechanical reliability, prominent electrical properties, and miniaturized size (compactness) for automotive applications.

Here, we develop a coiled CNT yarn harvester for harvesting rotational energy covering a wide speed range with stable power generation. This rotational harvester device can stably convert

This is an open access article under the CC BY-NC-ND license (http://creativecommons.org/licenses/by-nc-nd/4.0/).

rotational energy to repetitive tensile motions (stretch and release) of a coiled CNT yarn, which can generate electrical energy from wheel rotation during vehicle driving. The coiled CNT yarn harvester has a broad rotational speed covering up to a speed of 1,000 rpm and reliable performance that generates stable power with dynamic motion changes such as speed changes, quick start/stop motions, and external acceleration of impact, and stable power with environmental changes including variable humidity and temperature. For practical applications, we further show that a CNT harvester can harvest mechanical energy from rotational movement and charge it to a capacitor to provide energy.

RESULTS

REH based on CNT for automobile application

Figure 1A illustrates a rotational energy harvester device with a cylindrical disk shape that is comprised of a coiled CNT yarn as a harvesting electrode, solid electrolyte, inertial mass, rotating axis, and connecting rod. The coiled CNT yarn harvester consists of symmetrically connected CNT coiled yarns and solid electrolyte composed of 10% polyvinyl alcohol (PVA) and 0.6 M NaCl. Both ends of the harvesting unit with each CNT yarn were tethered and connected to the rotating axis with the connecting rod. The cylindrical-shaped inertial mass acts as a roller, which can minimize the frictional force between the mass and inner wall of the device surfaces, rolling along the rotating device (i.e., anti-clockwise direction) in the opposite direction (i.e., clockwise direction) and making it possible to sustain the stationary position of the harvesting unit even though the entire device revolves very fast. The harvester device is designed to be installed at the wheel hub, which includes the wheel's center axis, as shown as a schematic image in Figure 1A.

In our previous report,[41] we demonstrated not only stretching single CNT yarn as a working electrode but also simultaneously releasing the CNT yarn, which functions as a counter electrode. This configuration drastically enhances OCV generation, and we call this configuration a "seesaw structure," because of the opposite stretching phase of the working electrode and counter electrode like a seesaw.

In the general two-electrode system, a voltage between the working electrode and counter electrode is generated by the capacitance change that occurs when the CNT coiled yarn acting as the working electrode is stretched. Applying a "seesaw stretch and release phase" generates twice the voltage of stretching one CNT coiled yarn working electrode because of the two electrodes alternately acting as the working electrode and counter electrode, making the potential difference bigger between the working electrode and counter electrode. Specifically, in a two-electrode system using two coiled CNT yarns, the stretched coil acts as a working electrode and the released coil acts as a counter electrode. In summary, stretching both electrodes 180°-out-of-phase generates an approximately two times larger maximum OCV in the interelectrode than stretching only one electrode.

In order to apply this stretching phase to the electrode in a rotational harvester, we physically integrate the electrodes of a two-electrode system into a single one-body harvesting electrode for the volume of the harvesting system and simple strain applying structure, with electrical separation. Among the one-body electrode system, we named the upper CNT electrode as "yarn A" and the lower CNT electrode as "yarn B," shown in Figure 1A. The devised one-body harvesting electrode based on coiled CNT, which has a "seesaw" tendency of stretching phase, is described with harvested electron flow directions in Figures 1B–1D. In Figure 1B, the operating principle of the seesaw structure integrated into the rotational energy harvester is presented. The application of positive strain to "yarn A", acting as the harvesting electrode, results in an increase in its OCV, whereas an induced negative strain in "yarn B" causes a corresponding decrease in OCV. When "yarn A" and "yarn B" function as the working and counter electrodes, respectively, the oppositely directed OCVs collectively enhance the overall potential difference. The equivalent circuit model further illustrates that the capacitance is strain-dependent, and this mechanical modulation of capacitance is responsible for voltage generation. The coil electrodes were tethered as shown in Figure 1B, with red-colored end tethering for not to be stretched and torsioned, and green-colored tethering in the middle part of the coil is for strain-applying tethering which can move linearly freely but not rotate. In Figure 1C, when "yarn A" is stretched, electro double layer capacitance (EDLC) of the CNT electrode decreases as the electrolyte in the CNT electrode is squeezed out. Sequentially, directly connected "yarn B" is released, and EDLC of the electrode increases as the electrolyte is absorbed into the CNT coil. By the capacitance change occurring between two electrodes, potential difference is generated, and electrons flow from yarn A to yarn B, which work as anode and cathode, respectively. In Figure 1D, when the harvester rotates, electrons flow from yarn B to yarn A, which work as anode and cathode, respectively, as the voltage is generated by the capacitance change.

The principle of converting rotational energy to tensile force for reversible yarn stretching and release is discussed in detail below in Figure 1E. The rotating axis revolves around the wheel's center with a specific radius (R) and offers the displacement to the harvesting unit as a length of $2R$ through the connecting rod. For CNT yarns with a length L_0, which is fixed by the total size of the device, the coordinates of both ends of yarns A and B are A(R, L_0) and B(R, $-L_0$). The joint of two electrodes (point Rt) is moving on the edge of the circle with radius R proportional to the specific speed (frequency). In this regard, point Rt is dependent on the rotation angle (θ) and can be designated Rt ($R\cos\theta$, $R\sin\theta$), and θ is a function of time ($\theta = 2\pi ft$) with a frequency of f. As shown in Figure 1D, the yarn lengths of CNT "A" and "B" are the distances between points A and C and points B and C, respectively. Their lengths can be expressed by Equation 1 and 2.

$$L_A(\theta) = \sqrt{(R - R\cos\theta)^2 + (L_0 - R\sin\theta)^2} \quad \text{(Equation 1)}$$

$$L_B(\theta) = \sqrt{(R - R\cos\theta)^2 + (L_0 + R\sin\theta)^2} \quad \text{(Equation 2)}$$

These equations are derived by decomposing the yarn displacement into horizontal and vertical components, where

CellPress
OPEN ACCESS

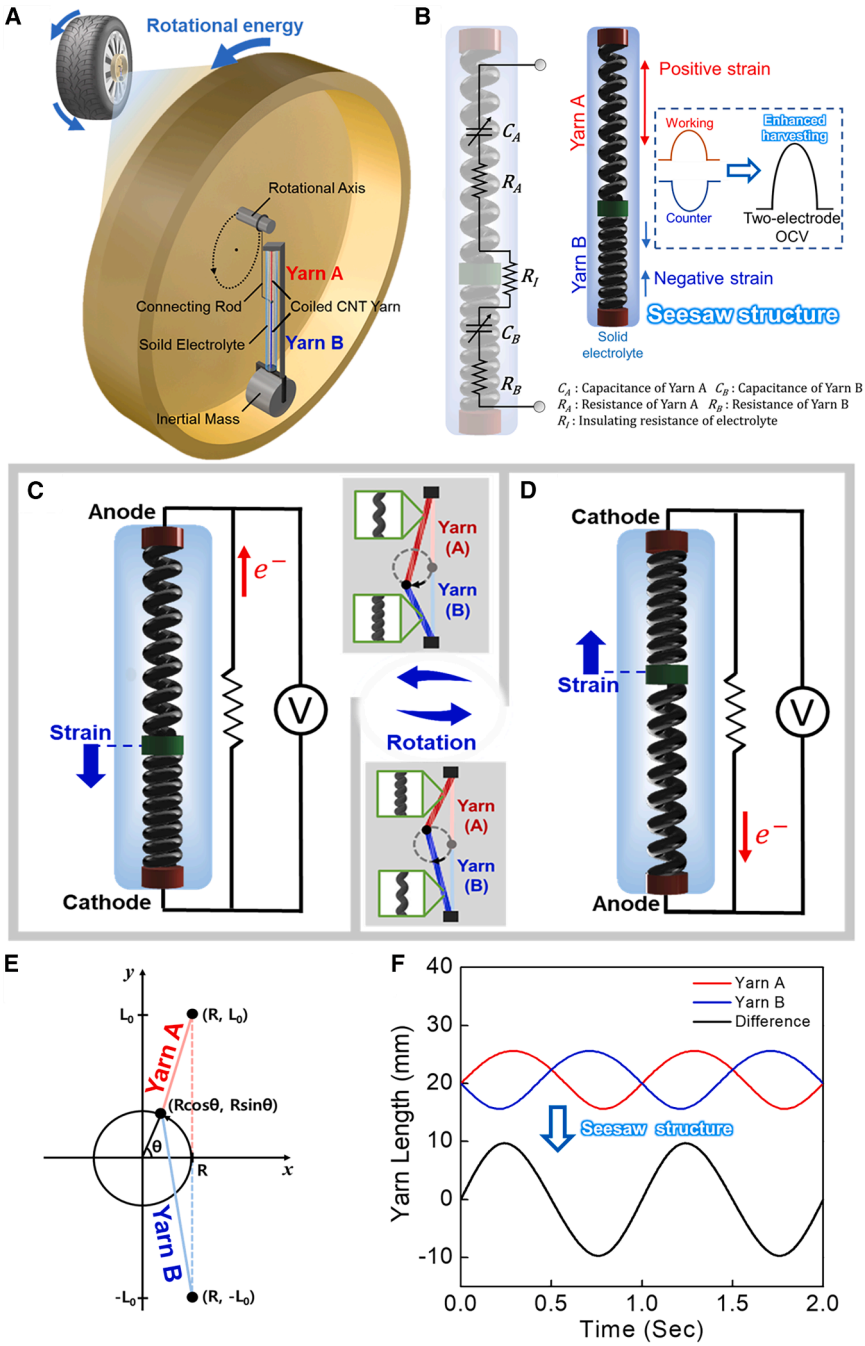

Figure 1. CNT-based rotational energy harvester for scavenging mechanical energy from rotating tires

(A) Schematic diagrams of rotational harvester device located on wheel hub, and device structure consists of coiled CNT yarn harvesters with solid electrolyte, rotational axis, inertial mass, and connecting rod.

(B) Equivalent circuit diagram of harvester and illustration of harvesting effect of seesaw structured mechano-electrochemical harvester.

(C and D) Illustration of harvesting principle of the rotational harvesting electrode and equivalent circuit diagram. (Inset) Schematic image of stretching state of the seesaw structured harvester electrodes.

(E) Schematic used to determine the coordination for relation of length changes of CNT yarns in rotational harvester.

(F) Dynamic length change for two CNT yarns and length difference of rotational harvesting electrode for one rotation cycle.

the horizontal term contributes equally to both yarns, while the vertical term introduces an opposite-phase variation of $\pm R\sin\theta$. The time-dependent length of coiled CNT yarns can be calculated with the above equations using the initial length (L_0), radius of the rotating axis (R), and frequency-dependent rotation angle (θ).

Using the definition of tensile strain,

$$\varepsilon(\theta) = \frac{L(\theta) - L_0}{L_0}, \qquad \text{(Equation 3)}$$

the strains of yarn "A" and "B" are obtained as

$$\varepsilon_A(\theta) = \frac{1}{L_0}\left[\sqrt{(R - R\cos\theta)^2 + (L_0 - R\sin\theta)^2} - L_0\right] \qquad \text{(Equation 4)}$$

$$\varepsilon_B(\theta) = \frac{1}{L_0}\left[\sqrt{(R - R\cos\theta)^2 + (L_0 + R\sin\theta)^2} - L_0\right]. \qquad \text{(Equation 5)}$$

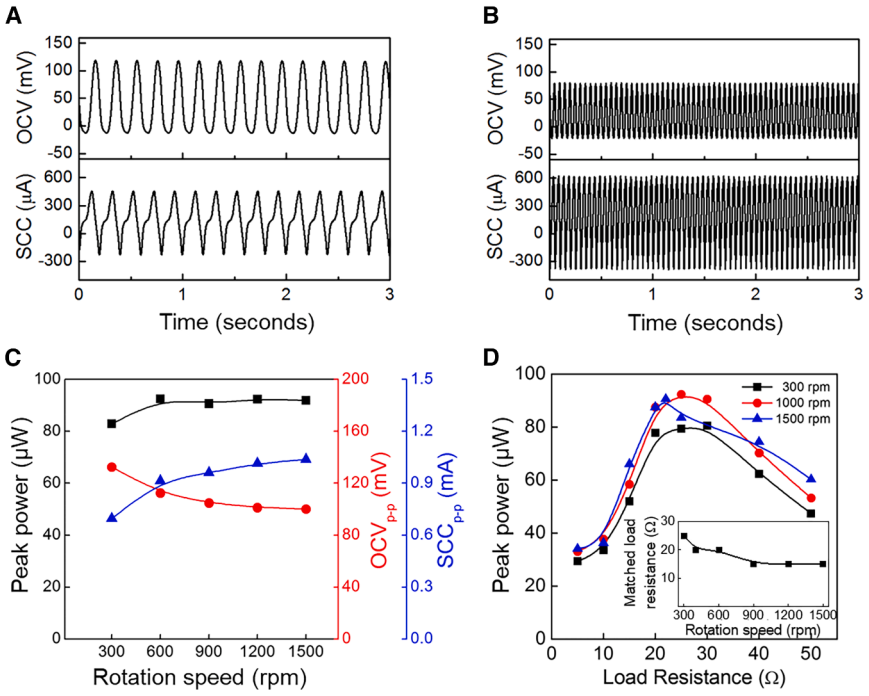

Figure 2. Energy harvesting characteristics at various rotation speeds for rotational harvester device based on CNT

(A and B) Dynamic OCV, SCC changes at (A) 300 and (B) 1,500 rpm of rotation speeds, respectively.

(C) Rotation speed dependence of OCV_{p-p}, SCC_{p-p}, and peak power (red circles, blue triangles, and black squares).

(D) Relationship between peak power and matched impedance with external load resistance at various rotation speeds. Inset figure shows the matched impedance with external load resistance, which maximizes the peak power at each rotation speed.

Figure 1F shows each length change of both CNT yarns while rotating at L_0 = 20 mm, R = 5 mm and f = 1 Hz. The change in the length of each coiled yarn varies sinusoidally with an amplitude of 2R, and their phase difference is nearly 180°. In addition, yarns A and B show a sinusoidal variation in the length change of yarn with a 2 times higher value of $4R$ as shown as the graph of length change difference in Figure 1F by applying opposite stretching phase of dual electrodes, which is deriving higher voltage generation. Initial yarn length and radius of rotating axis are 20 mm and 5 mm, respectively. Specific stretched and released state along the rotation angle is described in the inset scheme of Figure S1.

To maximize the energy harvesting performance, we optimized the length of the axis radius and the weight of the inertial mass of the coiled CNT yarn harvester. Figure S2A shows the energy harvesting performance according to the changes in the axis radius of the rotating axis. As the axis radius increases, the peak-to-peak OCV (OCV_{p-p}) and the generated peak power proportionally increase. In addition, Figure S2B shows the maximum operating speed at a certain mass. As the inertial mass increased, the maximum operating speed increased and saturated from over 30 g of mass. Based on this result, this device could operate at 1500 rpm of rotation speed when used at 30 g of mass, which suggests the ability to operate at the real vehicle speed of over 200 km/h, with an over 26-inch diameter of tire (calculated in Figure S4).

To characterize the energy harvester, we analyzed the energy harvesting performances of the rotational harvester device according to various rotation speeds. Figures 2A and 2B represent dynamic OCV and short circuit current (SCC) changes at rotation speeds of (a) 300 and (b) 1,500 rpm, respectively. The change in the OCV showed stable periodic sinusoidal variation from 300 to 1,500 rpm. Figure 2C shows the changes in the OCV_{p-p}, peak-to-peak SCC (SCC_{p-p}), and peak power when the rotation speed varied. The generation of OCV_{p-p} decreased, and conversely, SCC_{p-p} increased as the rotation speed increased. Hence, the generated peak power, which is the multiplication of voltage and current, appeared at a nearly constant level (80–90 μW) for rotation speeds ranging from 300 to 1,500 rpm. Moreover, Figure 2D represents the relationship between peak power and load resistance of external load at various rotation speeds. The inset of Figure 2D shows the maximum external load resistance at each rotation speed. In the speed range of 300–1,500 rpm, the maximum external loads appeared at 20–30 Ω, and this small change might be advantageous for the connection of external circuits or other devices required for electrical power supply (Table S1).

The harvesting stability of rotational harvester in automobile environment

For automobile applications, the rotational harvester should not only have sufficient harvesting performance but also be able to maintain reliable and durable harvesting stability despite changes in the external environment, such as vehicle speed, humidity, and temperature. As shown in Figure 2C above, we showed that the coiled CNT yarn harvester device exhibits a constant energy power within a broad rotation speed range. Furthermore, we examined the changes in the OCV while randomly varying the vehicle speed from 500 to 1,100 rpm. Figure 3A shows the changes in energy power generated at 510, 800, 660, and 1,120 rpm that are randomly changed within the vehicle speed suggested from the worldwide harmonized light vehicle test cycle (WLTC).[52–54] The peak-to-peak voltage (V_{p-p}) was measured at a fixed external load resistance of 25 ohm. The generated energy power was almost constant with dynamic speed changes while randomly changing from 510 to 1,120 rpm. Figure 3B shows the stable operation characteristics for the quick start/stop motion of the rotational device. Remarkably, the coiled CNT yarn harvester device showed a stable peak voltage generated for the repetitive sudden starting and stopping of the rotating device at 500 rpm.

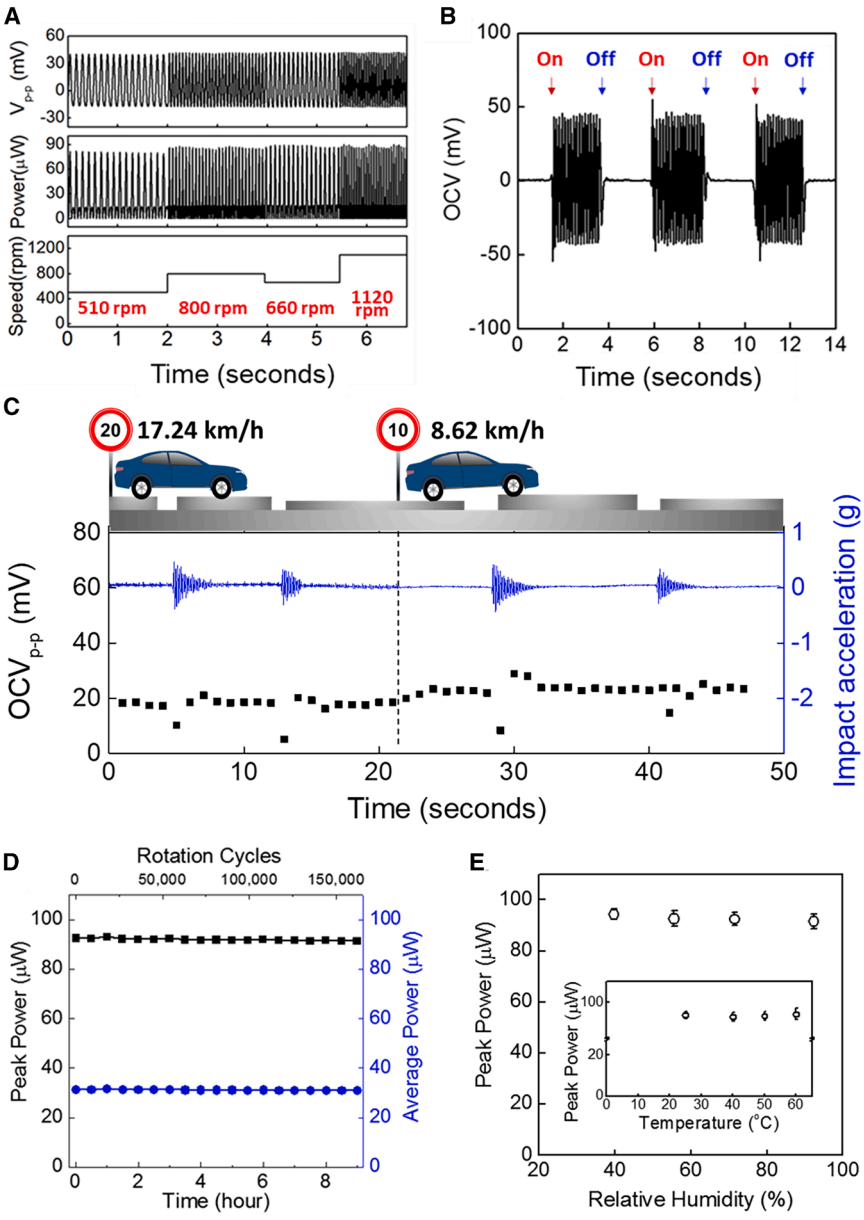

Figure 3. Performance of energy harvesting stability in an environment similar to real automobile

(A) Measured output voltage and generated power changes depend on dynamic speed variations. External load resistance was 30 ohm.

(B) Stable operating characteristics for quick start/stop motion of rotational harvester.

(C) Mechanical stability test by rotating harvester device when repeated impact acceleration was applied, simulating environment such as driving through pothole or off-road.

(D) Cycle test of harvester device at speed of 300 rpm.

(E) Environmental stability test with power generation performances for various conditions: humidity change and (inset) temperature change. The data points are represented as mean ± standard deviation.

Since automobiles can be driven on flat pavement and rough off-road environments, some experiments have been conducted to evaluate the mechanical durability of the vehicle like pothole tests, simulating arbitrary road surfaces.[55,56] When the car passes through the pothole, strong and sudden impact can be conveyed to the vehicle's wheels where our harvester device is installed, which can occasionally generate an acceleration in the vertical direction to a rotational harvester.[56] To simulate driving on a pothole, the entire experimental system, including the rotational harvester and rotational motor, was placed on the vibration table that can apply vibration in the vertical direction, as shown in Figure S3B. The schematic image in Figure 3C represents the simulation task of the vehicle's velocity and the road having arbitrary surface condition, including a pothole. To simulate the wheel clashing into the pothole while running at a certain speed, oscillation of the vertical direction caused by impact was applied by the vibration table, which applies maximum 3 cm of vertical displacements, causing high acceleration. In the simulation test, the rotational speeds were 240 and 120 rpm, which correspond to vehicle velocities of approximately 30 and 15 km/h, respectively, in regard to 25-inch height vehicle tire. Figure S4 shows the calculated relationship between vehicle driving and wheel rotating speeds for 25-inch size vehicle tire. From the linear relationship between the wheel rotation speed and the vehicle speed, the stretch and release speed of CNT yarn in the harvesting unit is dependent on the vehicle driving speed. As shown in Figure 3C, the OCV_{p-p} decreased when external impact was applied. This decreased OCV signal at an impact moment seems to be an altered distance caused by the inertial effect between the inner harvester unit and the outer shell of the harvester. The OCV generated from the harvester changes temporarily but immediately recovers to the original OCV_{p-p} value within approximately 3 s, regardless of rotating speed, showing the stable structure of the rotational harvester device, which is suitable for real application.

In addition, we further examined the durability and sustainability of the coiled CNT rotational harvester. For the long-term stability test, we measured the peak power at a rotational speed of 300 rpm for over 150,000 cycles (8 h). As a result, it was found that our rotational harvester device generates constant peak power and average power of approximately 94 and 31 μW for over 9 h, respectively (Figure 3D). This result indicates the prominent durability of our rotational harvester device to stably harvest

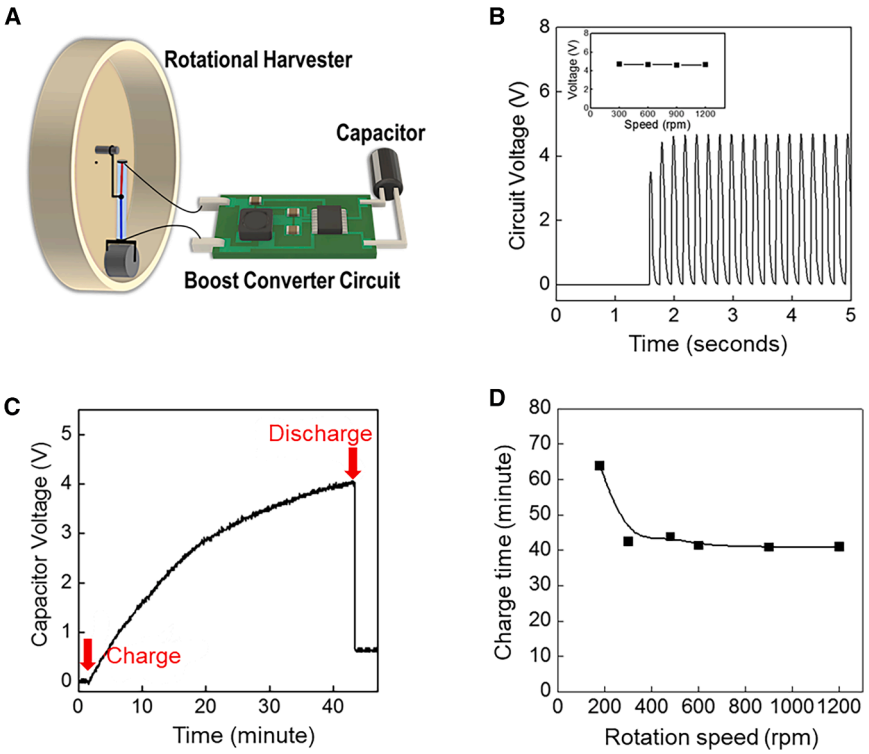

Figure 4. Power supplying and energy storage applications of the rotational harvester based on CNT for power storage

(A) Experimental setup for charging capacitor by rotational harvester.

(B) Measured voltage output from boost convert circuit. Operating rotation speed is 300 rpm.

(C) Measured voltages of a 1 mF commercial capacitor charged by the rotational harvester by rotating at 300 rpm. A 1 mF capacitor and boost convert circuit were electrically connected.

(D) The charging time of capacitor in conditions of various rotation speed.

electrical energy from rotational movement for over 150,000 cycles.

In addition to mechanical stability, stable harvesting performance is an important factor even in situations where the temperature and humidity change for real applications. As shown in Figure 3E, the peak power of our harvesting device was constantly generated at approximately 95 μW to increase the humidity from 40% to 80%. The test was performed in the chamber at a rotational speed of 300 rpm for 30 min under each humidity condition. Additionally, in Figure 3F, the peak power (96 μW) remained constant despite the temperature change from room temperature (20°C) to high temperature (60°C). The test was performed at a rotational speed of 300 rpm for 30 min at each temperature condition. Taken together, these results suggest that our harvester stably maintains energy harvesting performance under certain environmental changes, such as external shock and weather changes (humidity and temperature).

Power storage performance of rotational harvester based on CNT

To get one step closer to real application, the harvested energy from a rotational harvester should be charged to an energy storage system such as capacitor. Thus, we performed a test setup for a rotational harvester to charge a commercial capacitor as shown in Figure 4A. An experiment was conducted in which the electrical power from the harvester was received by the boost converter circuit shown in Figure S5, and the amplified voltage that passed through the boost converter circuit (LTC 3108, Linear Technologies) was stored in the capacitor. Correspondingly, Figure 4B presents the output voltage of the boost converter circuit that is amplified from the OCV output of the rotational harvester. Approximately 4.8 V of output voltage was measured constantly at a rotational speed of 300 rpm. The inset shows that the output voltage of the boost converter depends on the rotational speed of the harvester, indicating a negligible difference with the rotating speed. Figure 4C provides the result of charging 1 mF of a capacitor. The charged voltage of the capacitor according to the charging time shows the results of charging to 4.2 V for approximately 43 min at a rotational speed of 300 rpm. The correlation between the charging time and rotational speed of the harvesting device, which indicates the harvesting frequency, is shown in Figure 4D. The charging time begins to saturate from the experiment speed of 300 rpm, which is related to the OCV generated from the harvester.

DISCUSSION

In conclusion, we have developed a rotational energy harvester composed of two coiled one-body CNT yarns as a sustainable power source for automotive applications. To structurally maximize the generated voltage, we applied the seesaw configuration of two coiled CNT yarns to convert the rotation into linear motion. This coiled CNT-based rotational energy harvester covered a wide speed range (~1,500 rpm) and showed reliable and durable power generation in various simulated automobile environments, such as external impact, as well as humidity and temperature changes.

Remarkably, real-time monitoring devices using various sensors are considered to be important in transportation systems, including vehicles.[57] Among those, a tire pressure monitoring sensor (TPMS) on the vehicle's wheels has been a mandatory sensor for tire safety.[58] Since this possibility of being applicable to these real-time monitoring systems, further application experiment, including TPMS on the wheels of various vehicles with our rotational harvester, is expected to be attempted. Furthermore, experimental validation with the device directly mounted on an actual vehicle is necessary to confirm its feasibility under real driving conditions, including its durability and performance in

more practical operating environments.[59] In addition, incorporating previously reported strategies for high performance of mechano-electrochemical energy harvesting systems based on CNT into our electrode structure and device platform is expected to significantly enhance the harvesting power.[50,60–63] The improved output demonstration supports the feasibility of true self-powered applications for wireless sensor powering, and future work should focus on system-level integration and the operation of automotive sensors toward scalable self-powered sensing networks.[64]

METHODS

Materials

Spinnable multiwalled nanotube (MWNT) forest, which we use to produce CNT coiled harvesting electrode, was grown by chemical vapor deposition (CVD) method and purchased from A-TECH SYSTEM (Korea). Sodium chloride (NaCl; anhydrous, ACS reagent) and poly(vinyl alcohol) (PVA; Mw 146,000–186,000), used to fabricate 10 wt % PVA with 0.6 M NaCl as solid electrolytes, were purchased from Sigma-Aldrich (USA).

Fabrication process of rotational harvester and CNT electrode

The harvesting electrode of the rotational harvester was fabricated by cone spinning with a spinnable CNT forest shown in Figure S6. A 30-cm long and 5-cm-wide CNT sheet was pulled out from the CNT forest and rolled into a 1-cm-wide cylindrical shape for one of the CNT twisting methods called "cone spinning." The cylinder-shaped CNT sheet is twisted under a constant load with a twist density of approximately 600 turns/cm until it forms a coil structure with a spring index of 0.4–0.6. The spring index is calculated by $(D - d)/d$, where "D" is the outer diameter of the coil structured yarn, and "d" is the yarn diameter immediately before the onset of the formation of the coiled configuration. The fabrication process of rotational harvester device is shown in Figure S7. First, the rotational axis was located at the inner frame of the device, and it had the distance of the center axis of the device. Next, the middle of the CNT coiled yarn and the rotational axis were attached to the connecting rod, which is an unstretchable plastic part. The middle of the CNT yarn was electrically separated into two yarns, forming a working electrode and counter electrode, and the two separated yarns were connected to a plastic rod. Finally, an electrically separated but single one-body harvesting electrode was attached to the mass load, which was rolled on the inner wall of the device. Both ends of the harvesting electrode of CNT yarns were tethered and connected to the wire for measurement. The optical images of fabricated rotational harvester and harvesting electrode are shown in Figure S8.

Electrochemical characterization and acceleration measurement

The OCV was measured using a digital oscilloscope (InfiniiVision DSOX4024A, Keysight, USA) and the Gamry instrument (ref. 3000) open circuit voltage mode with a two-electrode system to test the harvesting device. External load resistance was connected to match impedance and measure power. The commercial acceleration sensor (PCB Piezotronics, 352C53) used to measure the applied impact acceleration is shown in Figure S3B.

RESOURCE AVAILABILITY

Lead contact

Requests for further information and resources should be directed to and will be fulfilled by the lead contact, Seon Jeong Kim (sjk@hanyang.ac.kr).

Materials availability

This study did not generate new unique reagents.

Data and code availability

- Data reported in this paper will be shared by the lead contact upon request.
- This paper does not report original code.
- Any additional information required to reanalyze the data reported in this paper is available from the lead contact upon request.

ACKNOWLEDGMENTS

This work was supported by the Nano & Material Technology Development Program through the National Research Foundation of Korea funded by Ministry of Science and ICT (RS-2024-00406534). This work was supported by the research fund of Hanyang University (HY-202500000000342).

AUTHOR CONTRIBUTIONS

Conceptualization, J.H.M. and B.-J.K.; methodology, J.H.M., T.J.M., and B.-J.K.; investigation, J.H.M., B.-J.K., and Y.J.; experiment, J.H.M., B.-J.K., G.H.S., S.Y., and D.K.; writing – original draft, J.H.M., B.-J.K., and Y.J.; writing – review and editing, J.H.M., B.-J.K., Y.J., and S.J.K.; funding acquisition, J.H.M. and S.J.K.; supervision, S.J.K.; J.H.M. and B.-J.K. contributed equally to this work.

DECLARATION OF INTERESTS

The authors declare no competing interests.

DECLARATION OF GENERATIVE AI AND AI-ASSISTED TECHNOLOGIES IN THE WRITING PROCESS

The authors declare no use of related tools.

SUPPLEMENTAL INFORMATION

Supplemental information can be found online at https://doi.org/10.1016/j.xcrp.2026.103263.

Received: October 20, 2025
Revised: January 20, 2026
Accepted: March 24, 2026
Published: April 21, 2026

REFERENCES

1. Mateu, L., and Moll, F. (2005). Review of energy harvesting techniques and applications for microelectronics. Proc. SPIE *5837*, 359–373.
2. Fan, K., Qu, H., Wu, Y., Wen, T., and Wang, F. (2020). Design and development of a rotational energy harvester for ultralow frequency vibrations and irregular human motions. Renew. Energy *156*, 1028–1039.
3. Ye, C., Wang, M., Min, J., Tay, R.Y., Lukas, H., Sempionatto, J.R., Li, J., Xu, C., and Gao, W. (2024). A wearable aptamer nanobiosensor for non-invasive female hormone monitoring. Nat. Nanotechnol. *19*, 330–337.

4. Kim, H., Rigo, B., Wong, G., Lee, Y.J., and Yeo, W.-H. (2023). Advances in wireless, batteryless, implantable electronics for real-time, continuous physiological monitoring. Nano-Micro Lett. *16*, 52.

5. Yuk, H., Lu, B., Lin, S., Qu, K., Xu, J., Luo, J., and Zhao, X. (2020). 3D printing of conducting polymers. Nat. Commun. *11*, 1604.

6. Yang, Y., Song, Y., Bo, X., Min, J., Pak, O.S., Zhu, L., Wang, M., Tu, J., Kogan, A., Zhang, H., et al. (2020). A laser-engraved wearable sensor for sensitive detection of uric acid and tyrosine in sweat. Nat. Biotechnol. *38*, 217–224.

7. Wang, Z., He, L., Gu, X., Yang, S., Wang, S., Wang, P., and Cheng, G. (2021). Rotational energy harvesting systems using piezoelectric materials: A review. Rev. Sci. Instrum. *92*, 041501.

8. Gielen, D., Boshell, F., and Saygin, D. (2016). Climate and energy challenges for materials science. Nat. Mater. *15*, 117–120.

9. Nag, A., Simorangkir, R.B.V.B., Sapra, S., Buckley, J.L., O'Flynn, B., Liu, Z., and Mukhopadhyay, S.C. (2021). Reduced graphene oxide for the development of wearable mechanical energy-harvesters: A review. IEEE Sens. J. *21*, 26415–26425.

10. Fan, K., Liu, J., Wei, D., Zhang, D., Zhang, Y., and Tao, K. (2021). A cantilever-plucked and vibration-driven rotational energy harvester with high electric outputs. Energy Convers. Manag. *244*, 114504.

11. Liu, A., Long, Y., Li, J., Gu, L., Karim, A., Wang, X., and Gibson, A.L.F. (2021). Accelerated complete human skin architecture restoration after wounding by nanogenerator-driven electrostimulation. J. Nanobiotechnol. *19*, 280.

12. Wu, N., Bao, B., and Wang, Q. (2021). Review on engineering structural designs for efficient piezoelectric energy harvesting to obtain high power output. Eng. Struct. *235*, 112068.

13. Pan, H., Qi, L., Zhang, Z., and Yan, J. (2021). Kinetic energy harvesting technologies for applications in land transportation: A comprehensive review. Appl. Energy *286*, 116518.

14. Kim, S., Choi, S.J., Zhao, K., Yang, H., Gobbi, G., Zhang, S., and Li, J. (2016). Electrochemically driven mechanical energy harvesting. Nat. Commun. *7*, 10146.

15. Fu, H., Mei, X., Yurchenko, D., Zhou, S., Theodossiades, S., Nakano, K., and Yeatman, E.M. (2021). Rotational energy harvesting for self-powered sensing. Joule *5*, 1074–1118.

16. Zhao, L.-C., Zou, H.-X., Zhao, Y.-J., Wu, Z.-Y., Liu, F.-R., Wei, K.-X., and Zhang, W.-M. (2022). Hybrid energy harvesting for self-powered rotor condition monitoring using maximal utilization strategy in structural space and operation process. Appl. Energy *314*, 118983.

17. Wang, X., Wang, Z.L., and Yang, Y. (2016). Hybridized nanogenerator for simultaneously scavenging mechanical and thermal energies by electromagnetic-triboelectric-thermoelectric effects. Nano Energy *26*, 164–171.

18. Zhang, Y., Luo, A., Wang, Y., Dai, X., Lu, Y., and Wang, F. (2020). Rotational electromagnetic energy harvester for human motion application at low frequency. Appl. Phys. Lett. *116*, 053902.

19. Zou, H.-X., Qin, N., Gan, C.-Z., Chen, Z.-W., Zhao, L.-C., Gao, Q.-H., Wei, K.-X., Meng, G., and Bai, Q. (2025). Human-friendly biomechanical energy harvesting vest for self-powered disability assistance functions. Energy *330*, 136863.

20. Bai, Q., Gan, C.-Z., Zhou, T., Du, Z.-C., Wang, J.-H., Wang, Q., Wei, K.-X., and Zou, H.-X. (2024). A triboelectric-piezoelectric-electromagnetic hybrid wind energy harvester based on a snap-through bistable mechanism. Energy Convers. Manag. *306*, 118323.

21. Han, J., Feng, Y., Chen, P., Liang, X., Pang, H., Jiang, T., and Wang, Z.L. (2022). Wind-driven soft-contact rotary triboelectric nanogenerator based on rabbit fur with high performance and durability for smart farming. Adv. Funct. Mater. *32*, 2108580.

22. Xie, Y., Wang, S., Lin, L., Jing, Q., Lin, Z.-H., Niu, S., Wu, Z., and Wang, Z.L. (2013). Rotary triboelectric nanogenerator based on a hybridized mechanism for harvesting wind energy. ACS Nano *7*, 7119–7125.

23. Zhang, J., Fang, Z., Shu, C., Zhang, J., Zhang, Q., and Li, C. (2017). A rotational piezoelectric energy harvester for efficient wind energy harvesting. Sens. Actuators, A *262*, 123–129.

24. Xi, Y., Guo, H., Zi, Y., Li, X., Wang, J., Deng, J., Li, S., Hu, C., Cao, X., and Wang, Z.L. (2017). Multifunctional TENG for blue energy scavenging and self-powered wind-speed sensor. Adv. Energy Mater. *7*, 1602397.

25. Zhao, L.-C., Zou, H.-X., Yan, G., Liu, F.-R., Tan, T., Zhang, W.-M., Peng, Z.-K., and Meng, G. (2019). A water-proof magnetically coupled piezoelectric-electromagnetic hybrid wind energy harvester. Appl. Energy *239*, 735–746.

26. Zhao, C., Zhang, Q., Zhang, W., Du, X., Zhang, Y., Gong, S., Ren, K., Sun, Q., and Wang, Z.L. (2019). Hybrid piezo/triboelectric nanogenerator for highly efficient and stable rotation energy harvesting. Nano Energy *57*, 440–449.

27. Rahman, M.T., Salauddin, M., Maharjan, P., Rasel, M.S., Cho, H., and Park, J.Y. (2019). Natural wind-driven ultra-compact and highly efficient hybridized nanogenerator for self-sustained wireless environmental monitoring system. Nano Energy *57*, 256–268.

28. Li, X., Cao, Y., Yu, X., Xu, Y., Yang, Y., Liu, S., Cheng, T., and Wang, Z.L. (2022). Breeze-driven triboelectric nanogenerator for wind energy harvesting and application in smart agriculture. Appl. Energy *306*, 117977.

29. Tollefson, J. (2014). Blue energy. Nature *508*, 302–304.

30. Guo, H., Wen, Z., Zi, Y., Yeh, M.-H., Wang, J., Zhu, L., Hu, C., and Wang, Z.L. (2016). A water-proof triboelectric-electromagnetic hybrid generator for energy harvesting in harsh environments. Adv. Energy Mater. *6*, 1501593.

31. Maurya, D., Kumar, P., Khaleghian, S., Sriramdas, R., Kang, M.G., Kishore, R.A., Kumar, V., Song, H.-C., Park, J.M.J., Taheri, S., and Priya, S. (2018). Energy harvesting and strain sensing in smart tire for next generation autonomous vehicles. Appl. Energy *232*, 312–322.

32. Qian, J., Kim, D.-S., and Lee, D.-W. (2018). On-vehicle triboelectric nanogenerator enabled self-powered sensor for tire pressure monitoring. Nano Energy *49*, 126–136.

33. Chen, J., Guo, H., Liu, G., Wang, X., Xi, Y., Javed, M.S., and Hu, C. (2017). A fully-packaged and robust hybridized generator for harvesting vertical rotation energy in broad frequency band and building up self-powered wireless systems. Nano Energy *33*, 508–514.

34. Nguyen, V., and Yang, R. (2013). Effect of humidity and pressure on the triboelectric nanogenerator. Nano Energy *2*, 604–608.

35. Gao, S., Han, Q., Jiang, Z., Zhang, X., Pennacchi, P., and Chu, F. (2022). Triboelectric based high-precision self-powering cage skidding sensor and application on main bearing of jet engine. Nano Energy *99*, 107387.

36. Gu, L., and Livermore, C. (2012). Compact passively self-tuning energy harvesting for rotating applications. Smart Mater. Struct. *21*, 015002.

37. Rui, X., Zhang, Y., Zeng, Z., Yue, G., Huang, X., and Li, J. (2021). Design and analysis of a broadband three-beam impact piezoelectric energy harvester for low-frequency rotational motion. Mech. Syst. Signal Process. *149*, 107307.

38. Fang, S., Wang, S., Miao, G., Zhou, S., Yang, Z., Mei, X., and Liao, W.H. (2020). Comprehensive theoretical and experimental investigation of the rotational impact energy harvester with the centrifugal softening effect. Nonlinear Dyn. *101*, 123–152.

39. Yang, Y., Shen, Q., Jin, J., Wang, Y., Qian, W., and Yuan, D. (2014). Rotational piezoelectric wind energy harvesting using impact-induced resonance. Appl. Phys. Lett. *105*, 053901.

40. Wang, Z., Qiu, H., Jiao, X., Wang, W., Zhang, Q., Tian, R., and Cao, D. (2024). Energy harvesting and speed sensing with a hybrid rotary generator for self-powered wireless monitoring. Acta Mech. Sin. *40*, 523508.

41. Kim, S.H., Haines, C.S., Li, N., Kim, K.J., Mun, T.J., Choi, C., Di, J., Oh, Y.J., Oviedo, J.P., Bykova, J., et al. (2017). Harvesting electrical energy from carbon nanotube yarn twist. Science *357*, 773–778.

42. Foroughi, J., Spinks, G.M., Wallace, G.G., Oh, J., Kozlov, M.E., Fang, S., Mirfakhrai, T., Madden, J.D.W., Shin, M.K., Kim, S.J., and Baughman,

R.H. (2011). Torsional carbon nanotube artificial muscles. Science *334*, 494–497.

43. Lima, M.D., Li, N., Jung de Andrade, M., Fang, S., Oh, J., Spinks, G.M., Kozlov, M.E., Haines, C.S., Suh, D., Foroughi, J., et al. (2012). Electrically, chemically, and photonically powered torsional and tensile actuation of hybrid carbon nanotube yarn muscles. Science *338*, 928–932.
44. Mun, T.J., Kim, S.H., Park, J.W., Moon, J.H., Jang, Y., Huynh, C., Baughman, R.H., and Kim, S.J. (2020). Wearable energy generating and storing textile based on carbon nanotube yarns. Adv. Funct. Mater. *30*, 2000411.
45. Kim, B.-J., Jang, Y., Moon, J.H., Baughman, R.H., and Kim, S.J. (2021). Self-powered carbon nanotube yarn for acceleration sensor application. IEEE Trans. Ind. Electron. *68*, 2676–2683.
46. Moon, J.H., Kim, B.-J., Jang, Y., Mun, T.J., Kim, H., and Kim, S.J. (2021). Self-powered inertial sensor based on carbon nanotube yarn. IEEE Trans. Ind. Electron. *68*, 8904–8910.
47. Jang, Y., Kim, S.M., Kim, K.J., Sim, H.J., Kim, B.-J., Park, J.W., Baughman, R.H., Ruhparwar, A., and Kim, S.J. (2019). Self-Powered Coiled Carbon-Nanotube Yarn Sensor for Gastric Electronics. ACS Sens. *4*, 2893–2899.
48. Lee, D.Y., Hyeon, J.S., Mun, T.J., Moon, J.H., Park, J.W., Kaner, R.B., and Kim, S.J. (2024). Synergistic effect of carbon nanotube yarn hybrid energy harvesters based on mechanical stretching and glucose. Adv. Mater. Technol. *9*, 2300920.
49. Moon, J.H., Gwac, H., Kim, K.W., Mun, T.J., Yoon, S., Choi, J., and Kim, S.J. (2025). Multifunctional CNT and nylon hybrid fibers for thermal artificial muscles and self-sensing without bias voltage. MRS Commun. *16*, 61–67.
50. Zhang, M., Cai, W., Wang, Z., Fang, S., Zhang, R., Lu, H., Aliev, A.E., Zakhidov, A.A., Huynh, C., Gao, E., et al. (2023). Mechanical energy harvesters with tensile efficiency of 17.4% and torsional efficiency of 22.4% based on homochirally plied carbon nanotube yarns. Nat. Energy *8*, 203–213.
51. Li, T., Jang, Y., Moon, J.H., Choi, J.G., Gwac, H., Lee, D.Y., Hyeon, J.S., Mun, T.J., Ahn, J.H., Jeong, Y., and Kim, S.J. (2024). Self-powered multidirectional strain sensor for electronic skin based on coiled carbon nanotube yarns. IEEE Sens. J. *24*, 2577–2587.
52. Zachiotis, A.T., and Giakoumis, E.G. (2021). Monte Carlo simulation methodology to assess the impact of ambient wind on emissions from a light-commercial vehicle running on the worldwide-harmonized light-duty vehicles test cycle (WLTC). Energies *14*, 661.
53. Tutuianu, M., Bonnel, P., Ciuffo, B., Haniu, T., Ichikawa, N., Marotta, A., Pavlovic, J., and Steven, H. (2015). Development of the world-wide harmonized light duty test cycle (WLTC) and a possible pathway for its introduction in the European legislation. Transp. Res. D *40*, 61–75.
54. Suarez-Bertoa, R., Zardini, A.A., Keuken, H., and Astorga, C. (2015). Impact of ethanol containing gasoline blends on emissions from a flex-fuel vehicle tested over the worldwide harmonized light duty test cycle (WLTC). Fuel *143*, 173–182.
55. Hu, H., and Zhong, Z. (2019). Explicit–implicit co-simulation techniques for dynamic responses of a passenger car on arbitrary road surfaces. Engineering *5*, 1171–1178.
56. Billal, M.K., Carneiro, G., Ozelo, R., and Kulkarni, M. (2015). Simulation of vehicle pothole test and techniques used. SAE Tech. Pap. *2015*, 1–9.
57. Pang, Y., Zhu, X., Lee, C., and Liu, S. (2022). Triboelectric nanogenerator as next-generation self-powered sensor for cooperative vehicle-infrastructure system. Nano Energy *97*, 107219.
58. Matsuzaki, R., and Todoroki, A. (2008). Wireless monitoring of automobile tires for intelligent tires. Sensors *8*, 8123–8138.
59. Zhang, Y., Zheng, R., Shimono, K., Kaizuka, T., and Nakano, K. (2016). Effectiveness testing of a piezoelectric energy harvester for an automobile wheel using stochastic resonance. Sensors *16*, 1727.
60. Song, G.H., Park, J.W., Moon, J.H., Lee, D.Y., Yoon, S., Kim, S.H., Choi, C., and Kim, S.J. (2025). Improvements in mechano-electrochemical energy harvesting performance of carbon nanotube yarns via poly(sodium 4-styrenesulfonate) coating. ACS Appl. Mater. Interfaces *17*, 54878–54887.
61. Gwac, H., Lee, D.Y., Song, G.H., Moon, J.H., Lee, J.M., Sim, H.J., Bang, J., Jeong, Y., Choi, C., and Kim, S.J. (2025). Enhanced mechanical and electrochemical properties of carbon nanotube fibers via embedded sucrose-derived porous carbon for mechanoelectrochemical energy harvesting. Adv. Funct. Mater. *36*, e14096.
62. Song, G.H., Lee, D.Y., Gwac, H., Moon, J.H., Hyeon, J.S., Choi, J., Kim, H., Jeong, Y., Choi, C., and Kim, S.J. (2025). Asymmetric Mechano-Electrochemical Energy Harvesting System with Surface Charge–Modified Carbon Nanotube Yarn for Wearable Devices. Small *21*, e08487.
63. Wang, Z., Mun, T.J., Machado, F.M., Moon, J.H., Fang, S., Aliev, A.E., Zhang, M., Cai, W., Mu, J., Hyeon, J.S., et al. (2022). More powerful twistron carbon nanotube yarn mechanical energy harvesters. Adv. Mater. *34*, e2201826.
64. Mun, T.J., Moon, J.H., Park, J.W., Baughman, R.H., and Kim, S.J. (2023). Environment-adaptable rotational energy harvesters based on nylon-core coiled carbon nanotube yarns. Small Methods *7*, 2300526.